

Supporting Information

Revealing the Effect of Substitutional Cation Doping in the A-site of Nanoscale APbI_3 Perovskite layers for Enhanced Retention and Endurance in Optoelectronic Resistive Switching for Non-Volatile Bipolar Memory Devices

*Twinkle George, and Arumugam Vadivel Murugan**

Advanced Functional Nanomaterials Research Laboratory,

Centre for Nanoscience and Technology, Madanjeet School of Green Energy Technologies,

Pondicherry University (A Central University),

Dr. R. Vankataraman Nagar, Kalapet, Puducherry-605014, India.

*Email:avmrajeshwar@gmail.com & avmurugan.nst@pondiuni.edu.in

Materials

Lead acetate trihydrate [$\text{Pb}(\text{CH}_3\text{COO})_2 \cdot 3\text{H}_2\text{O}$, 99%], formamidinium acetate ($\text{C}_3\text{H}_8\text{N}_2\text{O}_2$), were purchased from Sigma-Aldrich. Methylamine (CH_3NH_2 , 40 % in water), hydroiodic acid (HI, 57 % in water), N,N-dimethylformamide (DMF, anhydrous 99.9 %), dimethyl sulfoxide (DMSO, anhydrous 99.9%), cesium acetate [$\text{Cs}(\text{CH}_3\text{COO})$], were purchased from Alfa-Aesar, 2-propanol (IPA, 99 %) was purchased from Qualigens. These materials were used as such without further purification.

Characterizations

Rigaku Ultima IV X-ray diffractometer with Cu K α (1.5406 Å) radiation and 0.01° s $^{-1}$ scanning step size was utilized to confirm the structure and crystallinity of the as-synthesized APbI₃ metal halide perovskite powders. UV-2550 (Shimadzu, Japan) was utilized to achieve the optical characterization such as absorbance and diffused reflectance spectroscopy (DRS). Fourier transform infrared spectroscopy (FTIR) was obtained with the help of Thermo Nicolet (model 6700) with standard KBr pellet referencing. The thermal stability of the synthesized metal halide perovskites was learnt using the TG/DTA from TA instruments. The cross-sectional thickness of the device and the morphology of the APbI₃ powders was analyzed using Carl Zeiss Sigma. Elemental composition that was determined from the X-ray photo spectroscopy was relied upon the Thermo Scientific K-Alpha⁺ system, UK. The electrical switching performance was procured from Bio-Logic (SP-200) electrochemical work station, while for optical signals, Xenon lamp was utilized (Newport 150 W 96000 solar simulator).

Table S1. Theoritcal ionic radii for estimating the tolerance factor for the MW-ST synthesized APbI₃ (A=MA⁺, FA⁺, MAFA⁺, CsMA⁺, CsMAFA⁺) powder

Ions at the A-site, B-site and X-site	Ionic radii (pm)
MA ⁺	217
FA ⁺	253
Cs ⁺	167
Pb ²⁺	119
I ⁻	220

Taking the composition of the metal halide perovskite to be FA_xMA_yCs_{1-x-y}PbI₃, the tolrence factor was estimated using the formula,

$$t_{eff} = \frac{r_{cat} + r_{anion}}{\sqrt{2(r_{Pb^{2+}} + r_{anion})}},$$

where, $r_{cat} = xFA + yMA + (1 - x - y)Cs$

The octahedra tilting was extimated for the MW-ST synthesized APbI₃ metal halide perovskite powders using the relation,

$$\mu = \frac{r_{Pb^{2+}}}{r_I},$$

Where, $r_{Pb^{2+}}$ denoted the ionic radii of the Pb²⁺ anion, and r_I denotes the ionic radii of the iodide anion.

Table S2. Details of estimated tolerance factor values for the MW-ST synthesized APbI₃ (A=MA⁺, FA⁺, MAFA⁺, CsMA⁺, CsMAFA⁺) powders

A-site Cations	x	y	APbI ₃ perovskite	Goldschimt Tolerance factor (t)
MA ⁺	0	1	MAPI	0.916
FA ⁺	1	0	FAPI	0.986

MAFA ⁺	0.5	0.5	MAFAPI	0.949
CsMA ⁺	0	0.5	CsMAPI	0.859
CsMAFA ⁺	0.3	0.3	CsMAFAPI	0.857

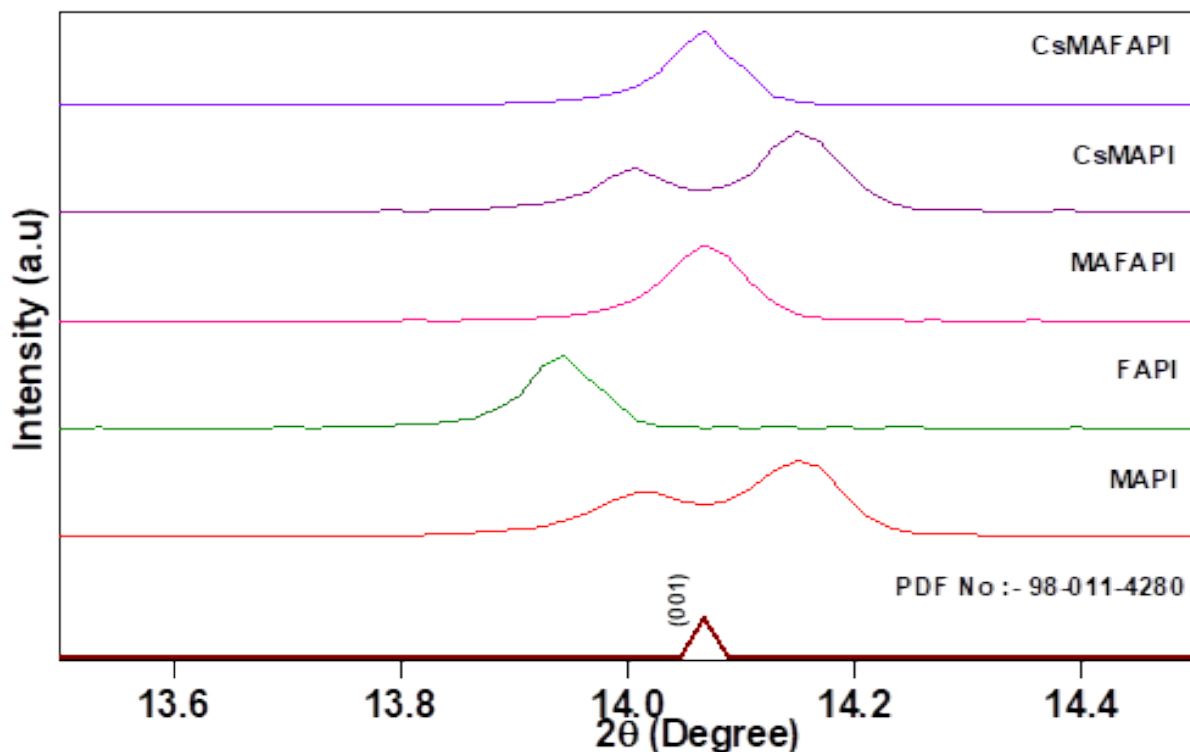


Fig S1 (a) Enlarged X-Ray diffraction pattern at 14° angle of (110) plane for the APbI₃ (A=MA⁺, FA⁺, MAFA⁺, CsMA⁺ and CsMAFA⁺) metal halide perovskites samples synthesized using MW-ST method

Table S3. Details of X-Ray diffraction pattern obtained for the MW-ST synthesized APbI₃ (A=MA⁺, FA⁺, MAFA⁺, CsMA⁺, CsMAFA⁺) powders

Sample Code	Crystalline Size (nm)	Lattice Parameters (Å)	Tetragonality	Unit Cell Volume (Å) ³
<i>a=b, c</i>				
MAPI	23.58	8.906, 12.6	1.414	999.4
FAPI	23.75	9.008, 12.74	1.414	1033.8
MAFAPI	23.82	8.932, 12.63	1.414	1007.6

CsMAPI	23.66	8.900, 12.58	1.413	996.5
CsMAFAPI	23.73	8.932, 12.63	1.414	1007.6

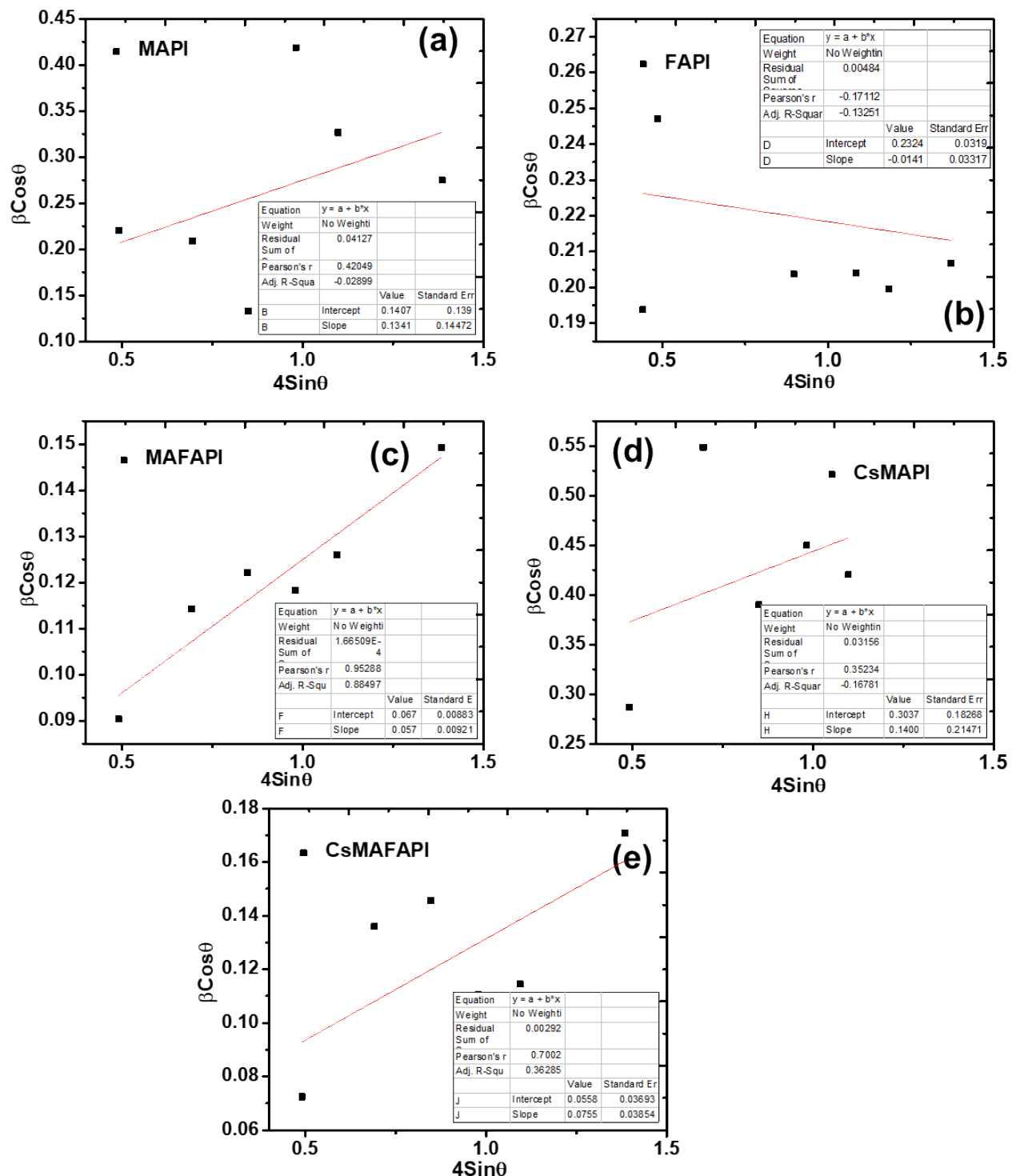


Fig S2. (a-e) Williamson-hall plot for the MW-ST synthesized APbI_3 ($A=\text{MA}^+$, FA^+ , MAFA^+ , and CsMA^+) metal halide perovskite powders under ambient conditions.

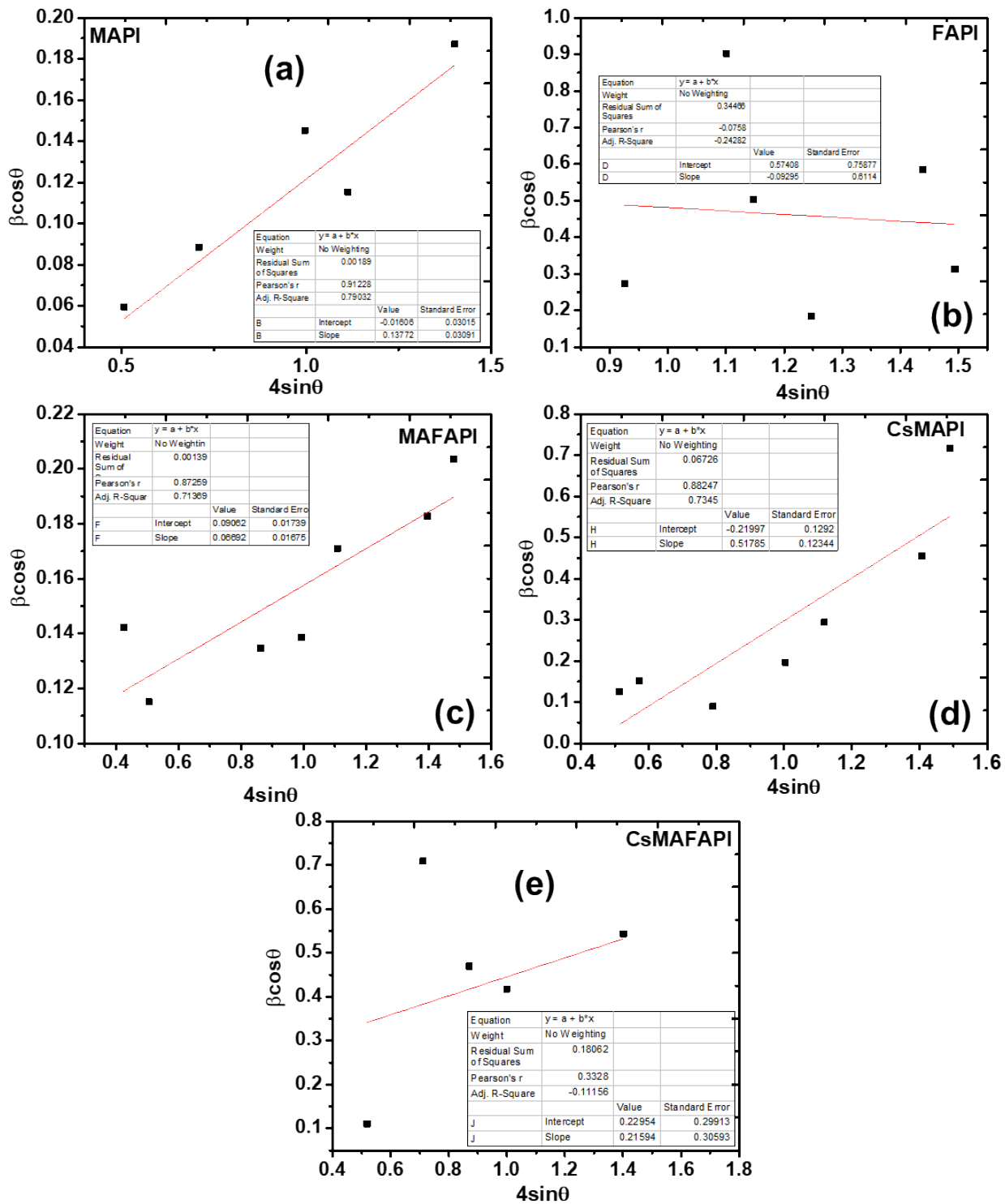


Fig S3. (a-e) Williamson-hall plot for the APbI_3 ($\text{A}=\text{MA}^+$, FA^+ , MAFA^+ , and CsMA^+) metal halide perovskite thin films based NVBRs memory devices.

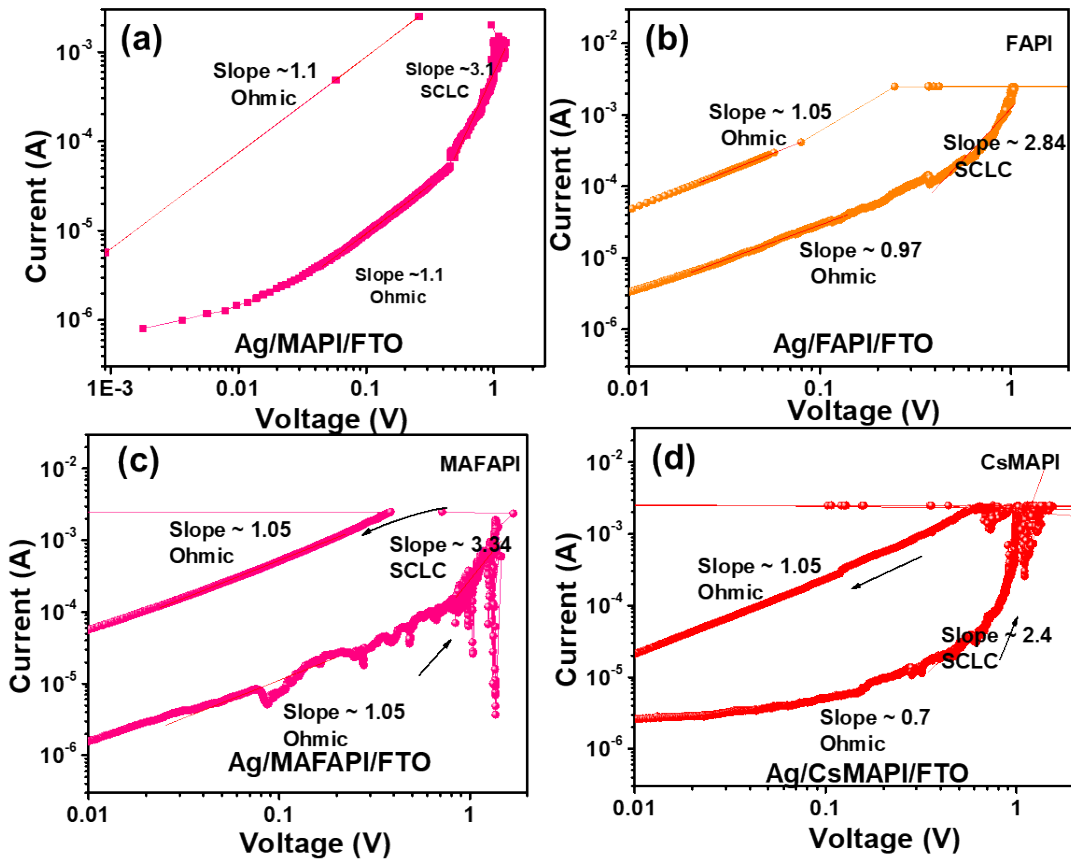


Fig S4. (a-d) logI-logV for determining the conduction mechanism of the APbI_3 ($\text{A}=\text{MA}^+$, FA^+ , MAFA^+ , and CsMA^+) metal halide perovskites thin films based NVBRS memory devices.

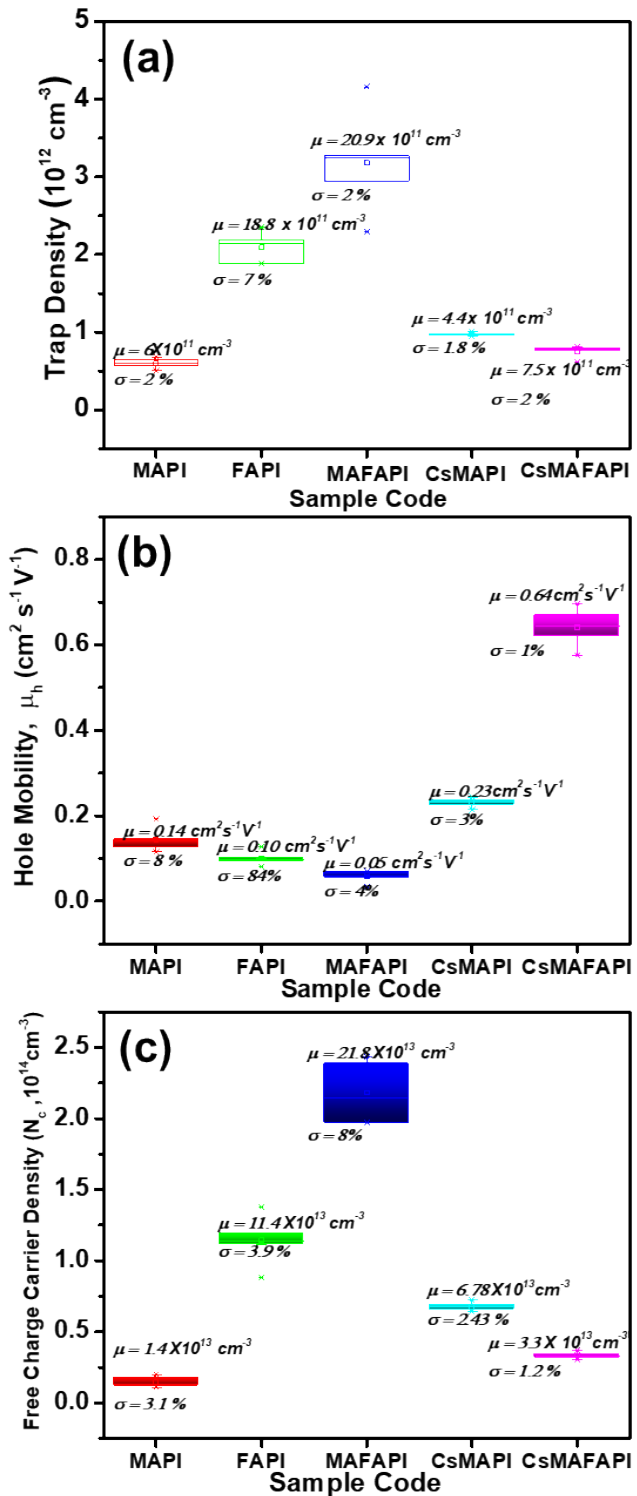


Fig S5. Statistical distribution taken from five different devices for (a) trap density (b) hole mobility and (c) free charge carrier density of the Ag/ABl₃/FTO (A=MA⁺, FA⁺, MAFA⁺, CsMA⁺ and CsMAFA⁺) based ORSNVB memory devices.

Table S4. Estimation of wave number, force constant and bond lengths for the MW-ST synthesized APbI₃ Perovskite (A=MA⁺, FA⁺, MAFA⁺, CsMA⁺ and CsMAFA)

Herein, $\mu = M_1M_2/M_1+M_2$,

Composition	MAPI		FAPI		MAFAPI		CsMAPI		CsMAFAPI	
	ρ (NH ₃) ⁺	γ (C-N)	ρ (NH ₃) ⁺	γ (C-N)	ρ (NH ₃) ⁺	γ (C-N)	ρ (NH ₃) ⁺	γ (C-N)	ρ (NH ₃) ⁺	γ (C-N)
Wave number (cm ⁻¹)	1243.26	993.6	-	987.7	1240.46	990.8	1231.6	981.7	1237.4	1002.5
Force Constant (N/cm)	0.87	2.03	-	2.03	0.86	2.03		2.02	0.86	2.04
Bond Length (Å)	2.69	2.03	-	2.03	2.69	2.03	2.7	2.03	2.69	2.02
Composition	MAPI		FAPI		MAFAPI		CsMAPI		CsMAFAPI	
	τ (NH ₂)	v_a (N-C-N)								
Wave number (cm ⁻¹)	696.8	-	699.8	1340.33	679.8	1343.36	696.2	-	688.2	1340.3
Force Constant (N/cm)	0.46	-	0.46	5.952	0.45	5.959	0.46	-	0.46	5.954
Bond Length (Å)	3.32	-	3.32	1.419	3.33	1.418	3.32	-	3.33	1.418

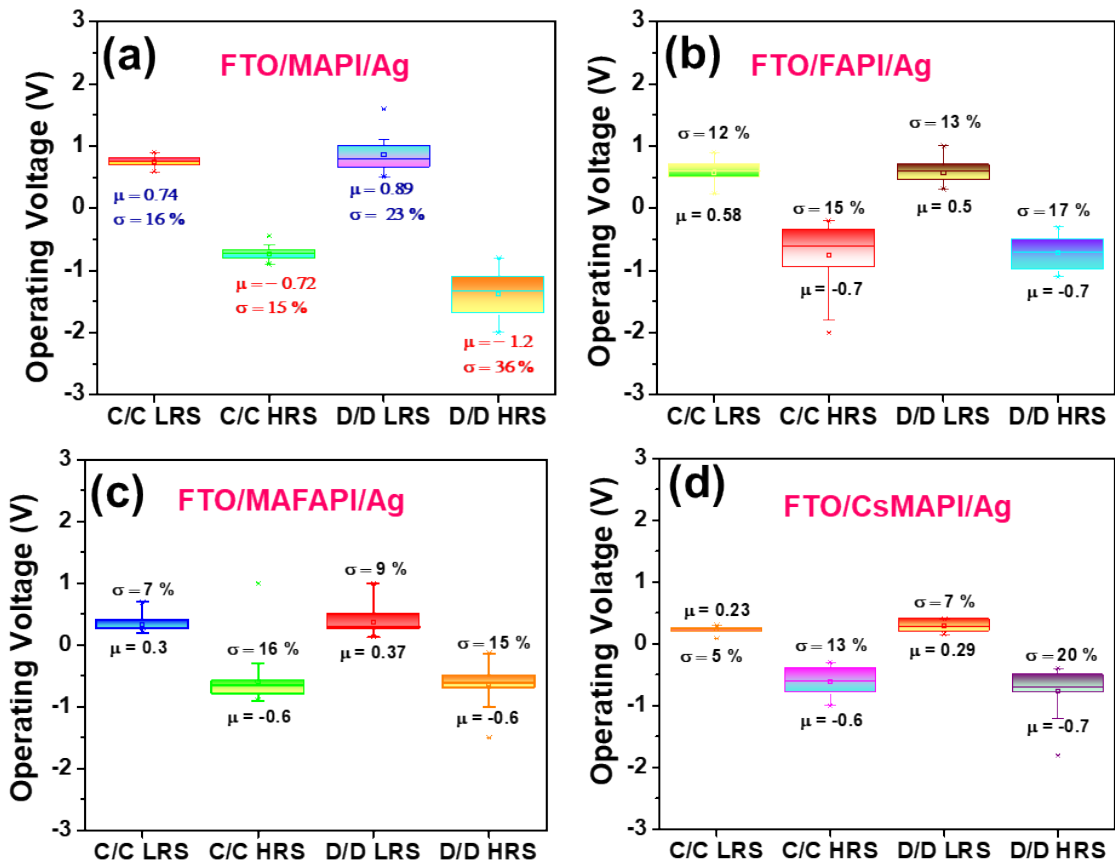


Fig S6. (a-d) Reliability of the APbI_3 ($\text{A}=\text{MA}^+$, FA^+ , MAFA^+ and CsMA^+) metal halide perovskite thin films based NVBRS devices shown using the statistical distribution of the variation in operational voltage as upon cycle-to-cycle (C/C) and device-to-device (D/D) performance

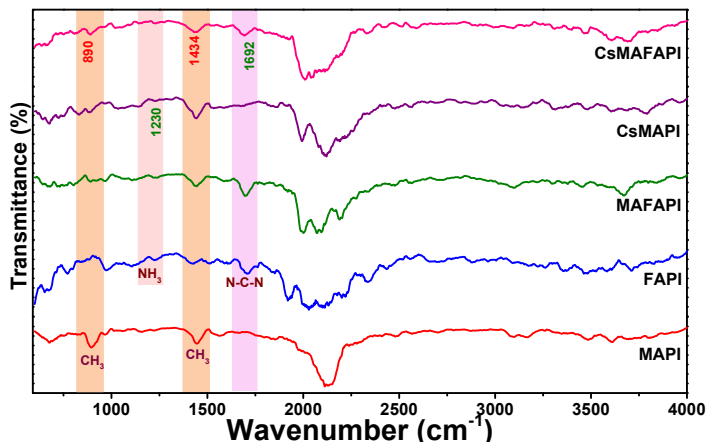


Fig S7. FTIR spectra for the APbI_3 ($\text{A}=\text{MA}^+$, FA^+ , MAFA^+ , CsMA^+ and CsMAFA^+) metal halide perovskites samples synthesized using MW-ST method after 5 months of storage in the dark

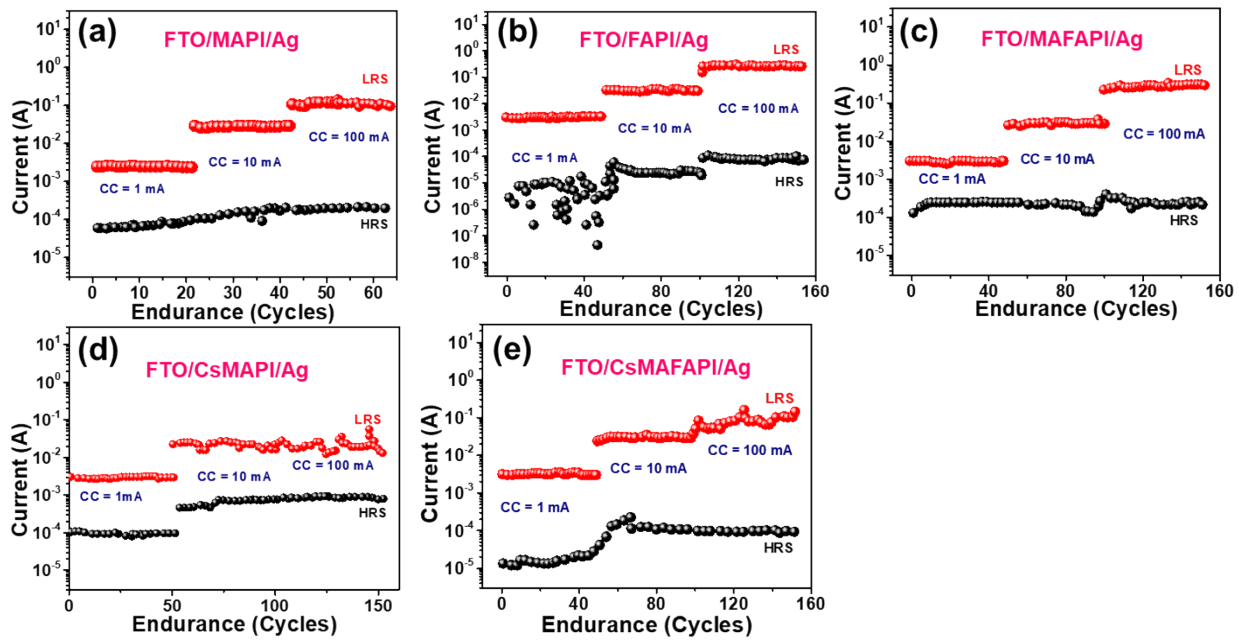


Fig S8. Compliance current based reliability performance of the APbI_3 ($\text{A}=\text{MA}^+$, FA^+ , MAFA^+ , CsMA^+ and CsMAFA^+) metal halide perovskites thin films based NVBRS memory devices.

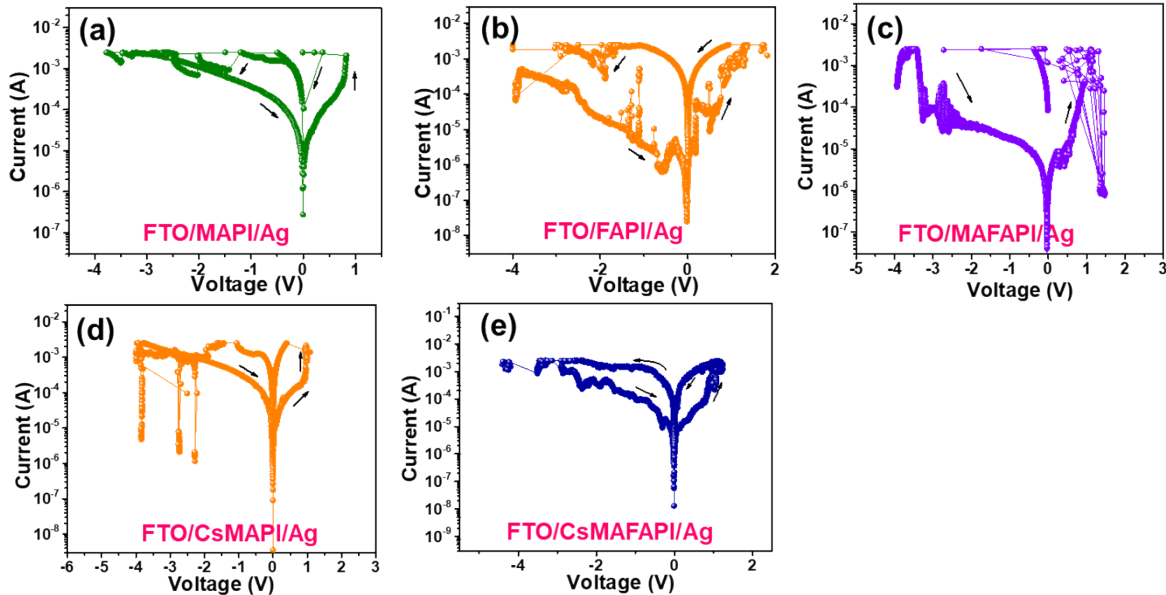


Fig S9. (a-e) Semi-logarithmic I-V graphs for the fabricated $\text{Ag/APbI}_3/\text{FTO}$ devices after 50 days of fabrication and storage in dark under ambient conditions.

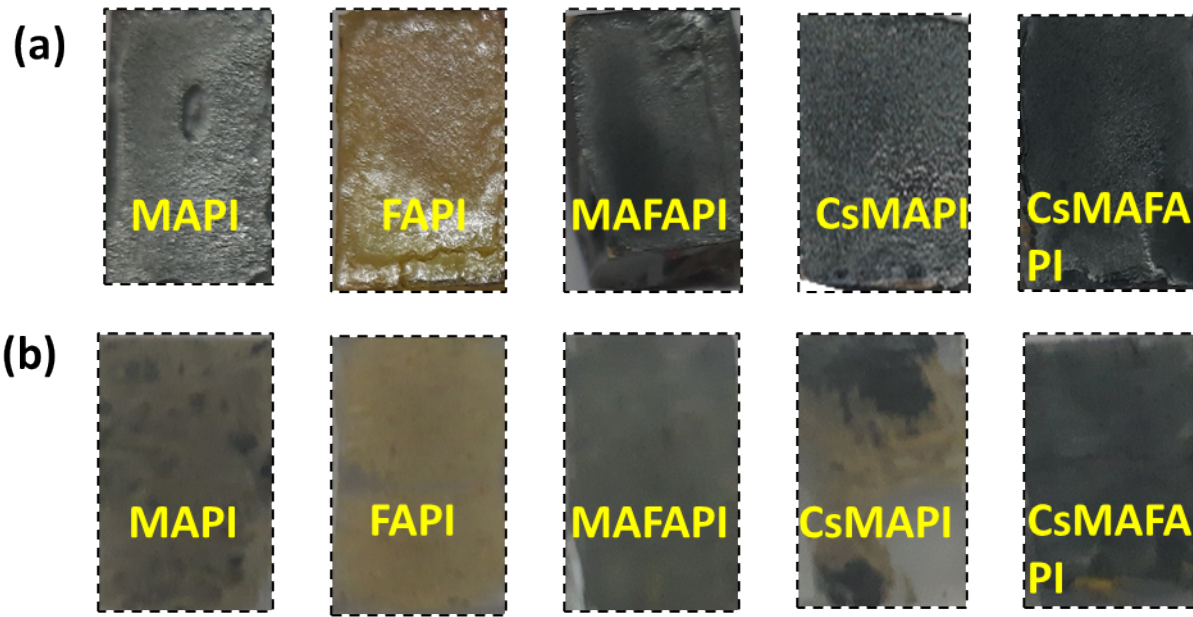


Fig S10. Photographs of the recrystallized nanoscale thin films of APbI_3 (A=) (a) immediately after annealing (b) after 5 month of storage in dark under ambient conditions.

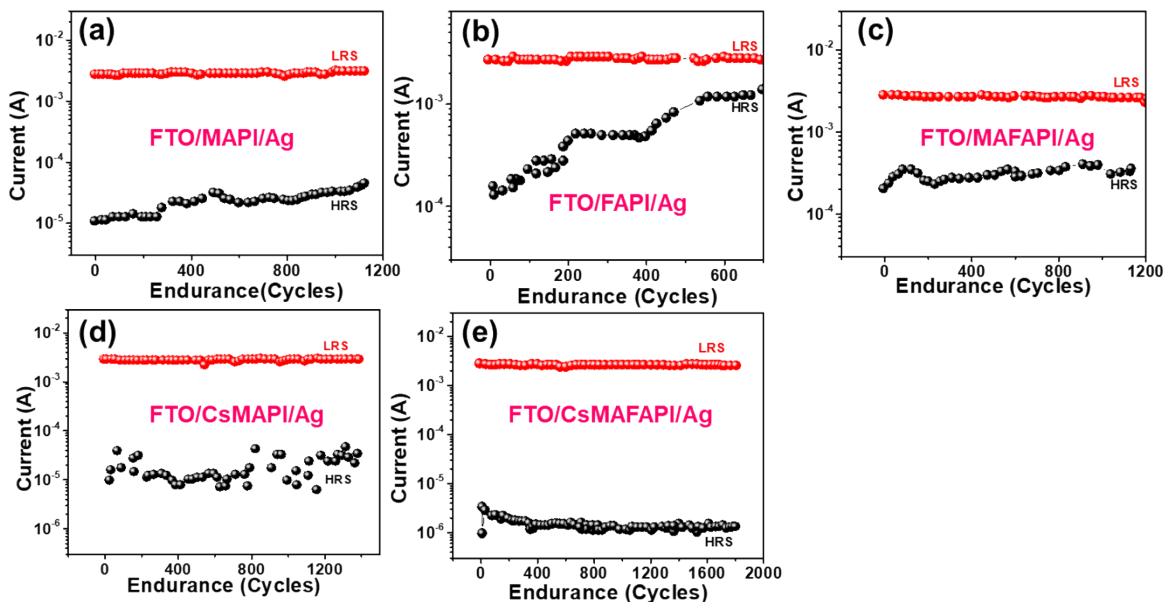


Fig S11. (a-e) Endurance performance of the APbI_3 ($\text{A}=\text{MA}^+$, FA^+ , MAFA^+ , CsMA^+ and CsMAFA^+) metal halide perovskite thin film based NVBRS memory devices under illumination.

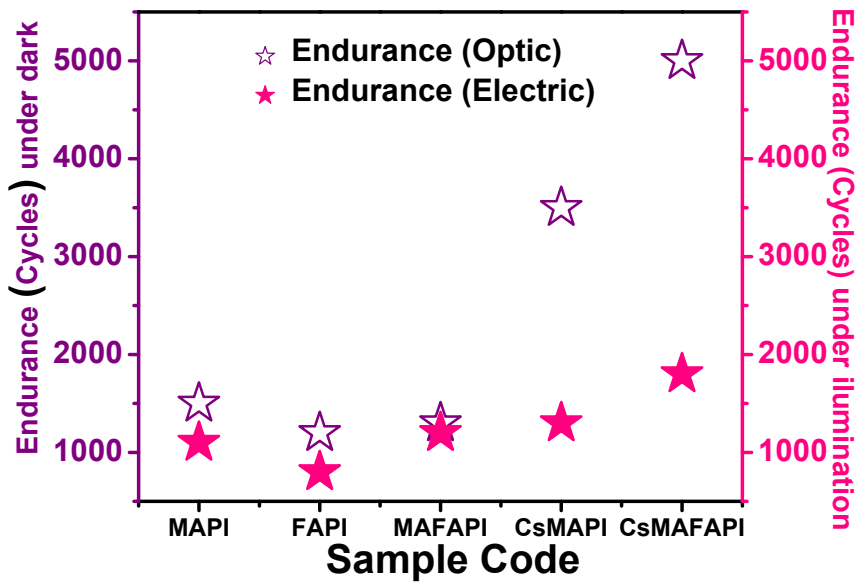


Fig S12. Comparison of variation in endurance with respect to electric signal and when illuminated.

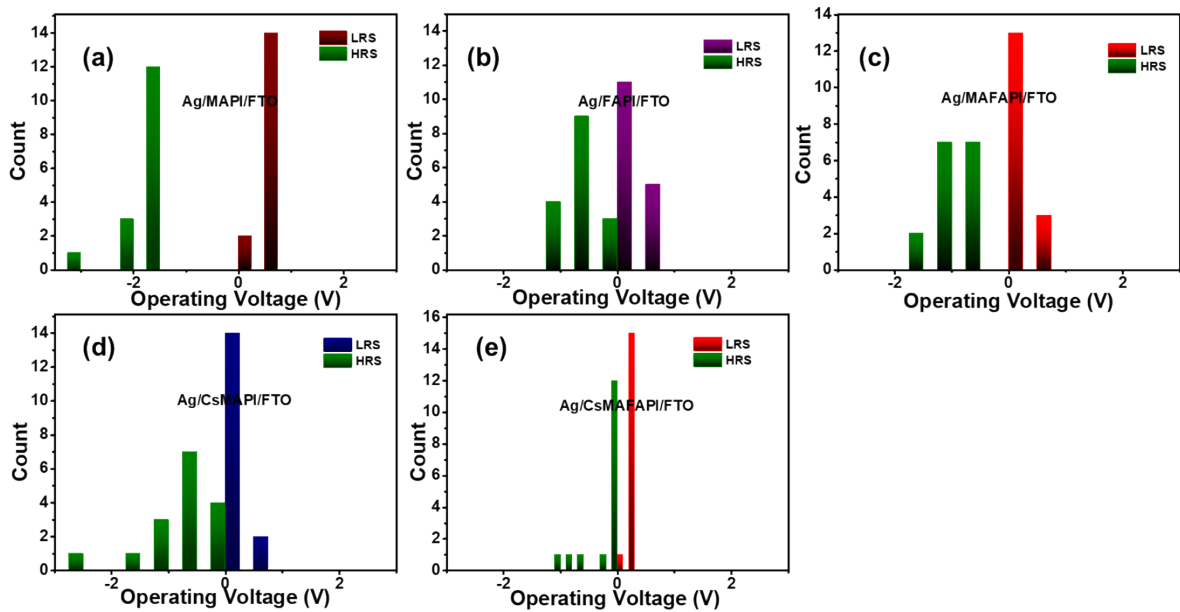


Fig S13. (a-e) Cumulative plot for variation in operational voltages with respect to various devices under illumination.

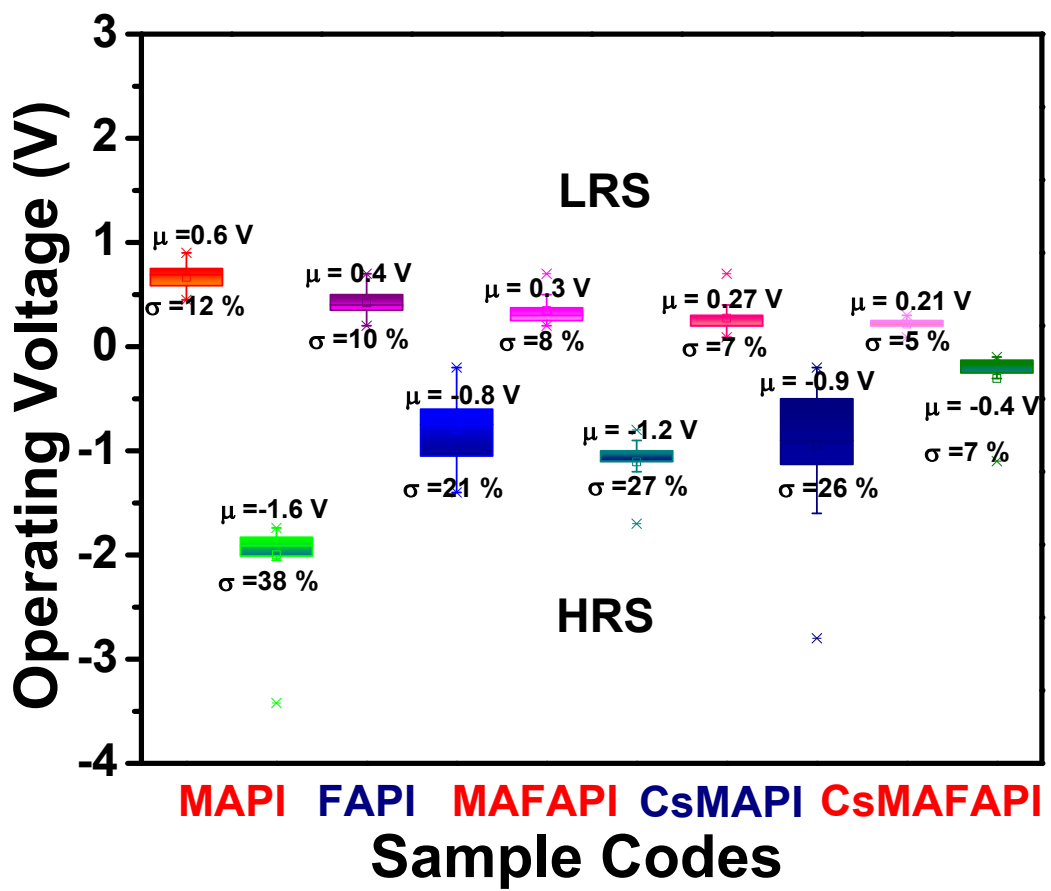


Fig S14. Statistical distribution of the operating voltages for the Ag/APbI₃/FTO (A=MA⁺, FA⁺, MAFA⁺, CsMA⁺ and CsMAFA⁺) memory devices under illumination.

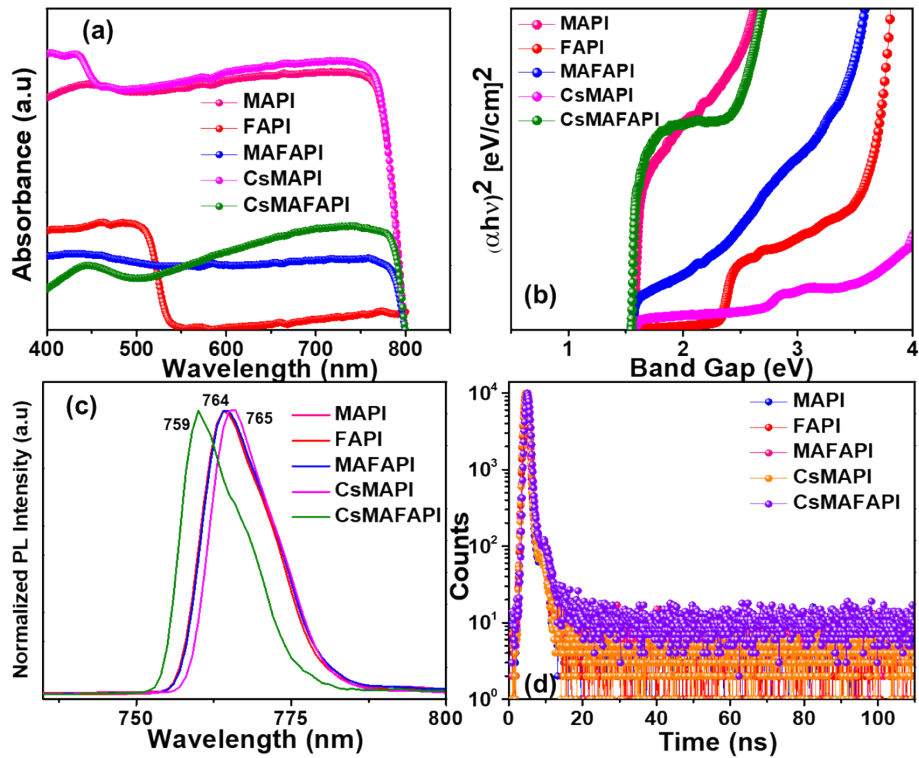


Fig S15. (a) UV-vis absorption spectra with (b) band gap determination using Tauc plot and (c) Steady-state PL spectra and (d) time-resolved PL spectra for the APbI_3 ($\text{A}=\text{MA}^+$, FA^+ , MAFA^+ , CsMA^+ and CsMAFA^+) metal halide perovskites samples synthesized using MW-ST method

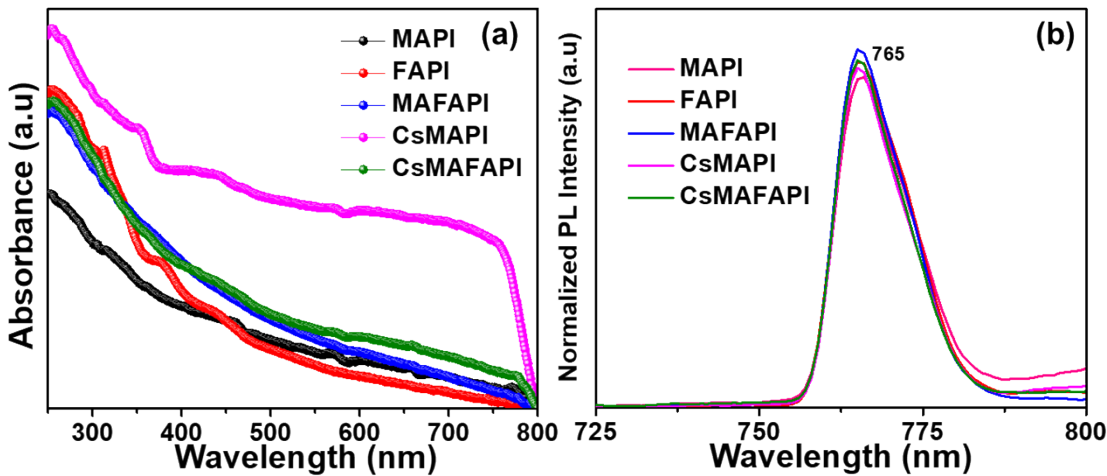


Fig S16. (a) UV-vis absorption spectra and (c) Steady-state PL spectra for the APbI_3 ($\text{A}=\text{MA}^+$, FA^+ , MAFA^+ , CsMA^+ and CsMAFA^+) metal halide perovskites thinfilms recrystallized on FTO via solution processed nanoscale self-assembly upon annealing at 120°C the precursor solution of the APbI_3 ($\text{A}=\text{MA}^+$, FA^+ , MAFA^+ , CsMA^+ and CsMAFA^+) powders dissolved in aprotic solvents DMF:DMSO (8:2).

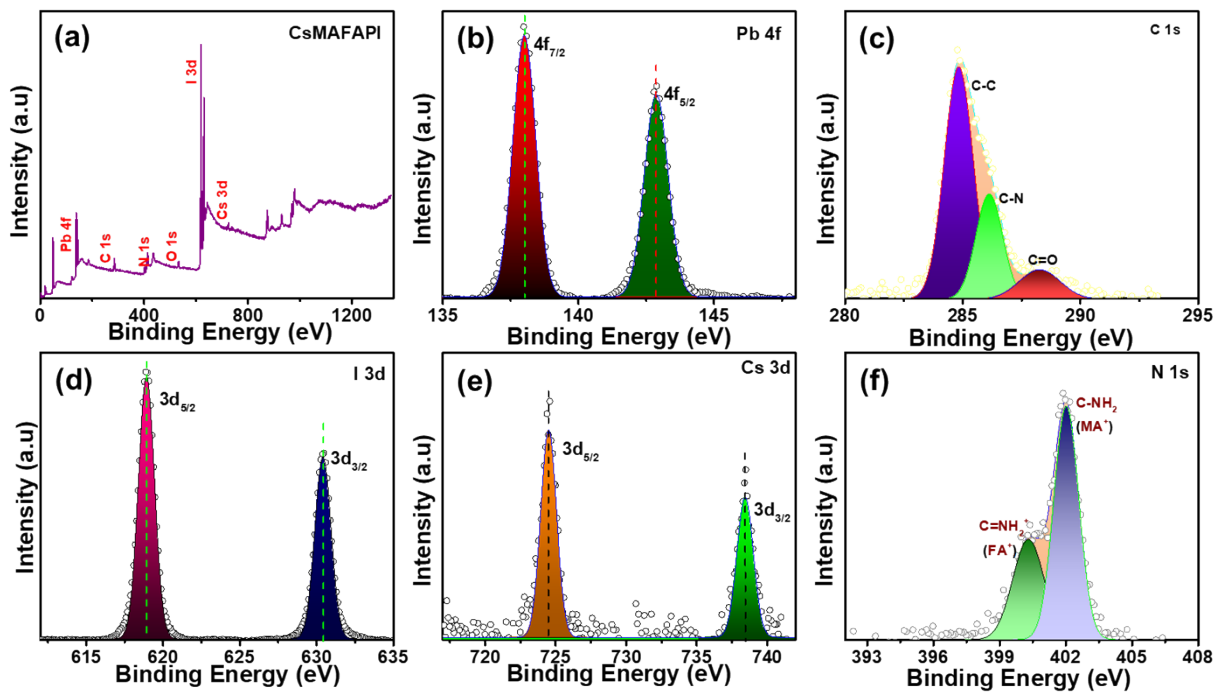


Fig S17. (a) XPS survey scan for CsMAFAPI thin film, with the core level spectra for (b) Pb 4 f (c) C 1 s (d) I 3d (e) Cs 3d and (f) N 1s.

XPS measurements were carried out for the CsMAFAPI thin film, **Fig S17 a** show the survey scan of the metal halide perovskite film. **Figure S17, b-f** depicts the narrow scan for each element present. The N 1s spectra shown in **Fig S17 f** is deconvoluted into two peaks associated with MA^+ and FA^+ at 400 and 402 eV. The dominance of the MA^+ cation is clearly visible by the relative intensity and areas, corroborating with the SEM morphology of cubes. Though equimolar precursors were used initially for the synthesis, the amount and composition of organic cation that can be accommodated in the octahedral framework is determined by the intercalation ability of the cation. Similarly, the C 1s deconvolution shows three peaks attributed by the influence of the cation. The C 1s peak at 285.5 eV can be associated with the CH_3I from the MA^+ cation, while, the high energy peak at 287.5 eV can be attributed to the C of FA^+ cation.

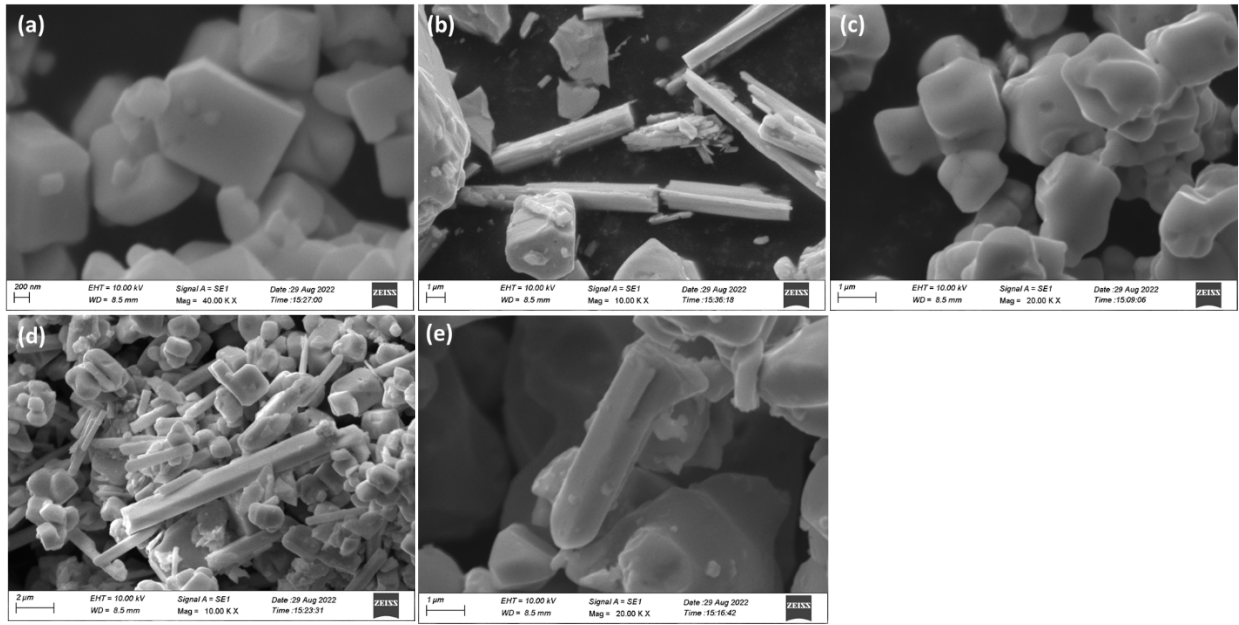


Fig S18. (a-e) SEM images of the as-synthesized APbI_3 ($\text{A}=\text{MA}^+, \text{FA}^+, \text{MAFA}^+, \text{CsMA}^+$ and CsMAFA^+) perovskite powders via MW-ST method.

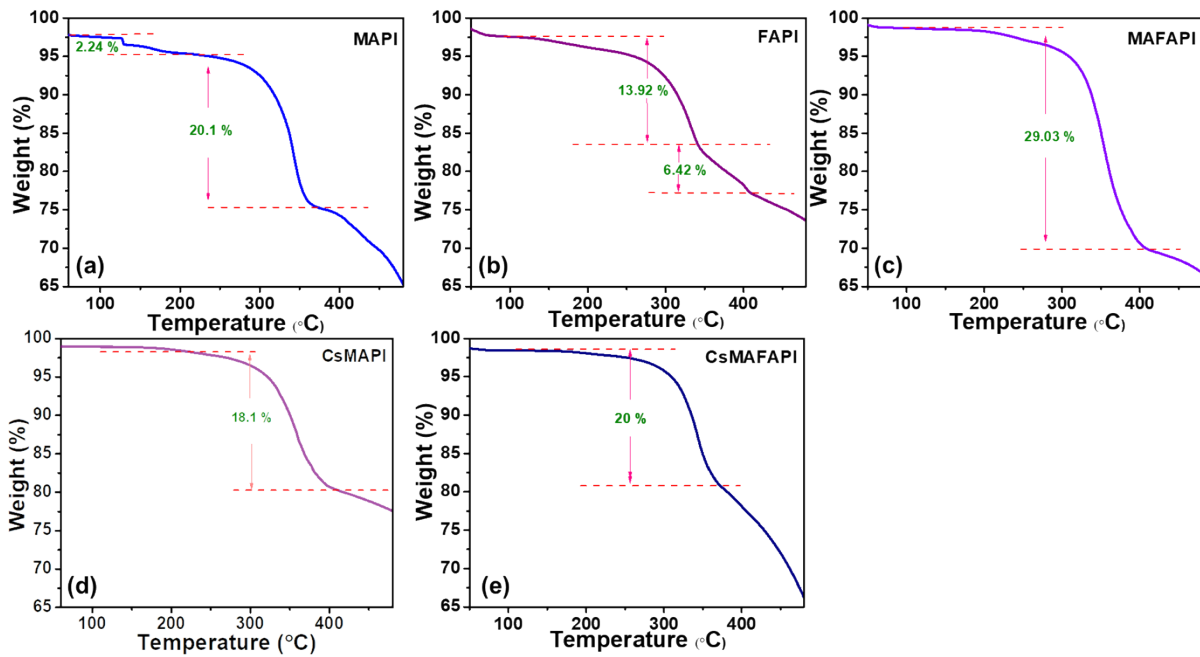


Fig S19. (a-e) TGA thermal analysis for the APbI_3 ($\text{A}=\text{MA}^+$, FA^+ , MAFA^+ , CsMA^+ and CsMAFA^+) metal halide perovskites samples synthesized using MW-ST method

Thermal analysis was carried out for the APbI_3 ($\text{A}=\text{MA}^+$, FA^+ , MAFA^+ , CsMA^+ , CsMAFA^+) metal halide perovskite powders from RT to 500 °C under ambient conditions. It could be observed that, the pure organic cation incorporated perovskites MAPI, FAPI and MAFAPI shows multiple degradation denoting the weak bonding between the organic moieties and the inorganic PbI_6 octahedra cage. However, in the case of incorporation of the inorganic cation Cs^+ both CsMAPI and CsMAFAPI shows continuous mass loss after 350 °C, depicting the strong coordination and stability of the material.

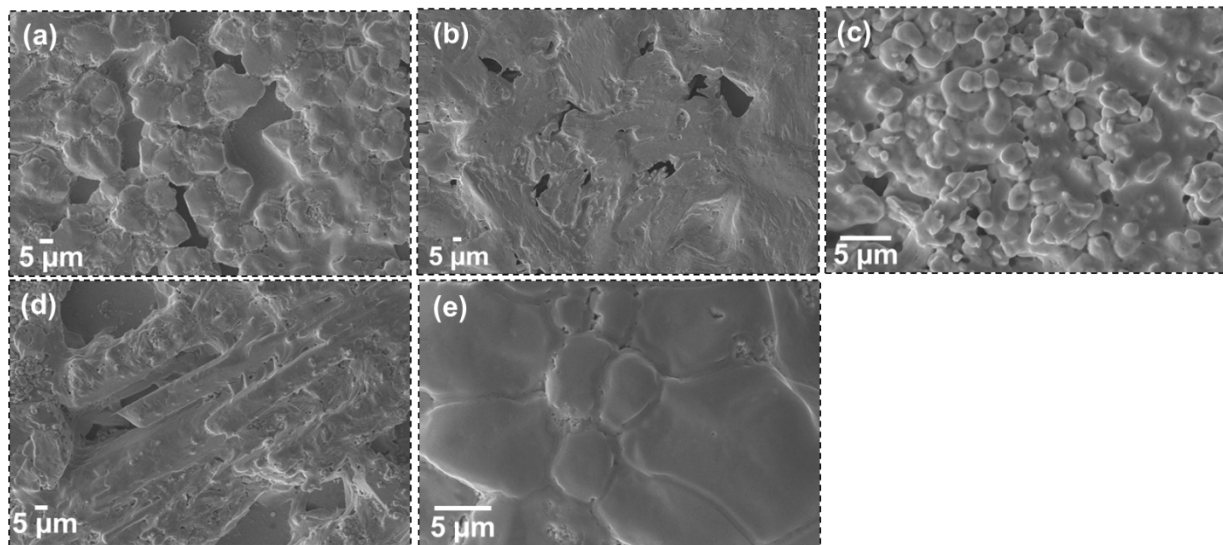


Fig S20. (a-e) SEM surface topography of the as-prepared nanoscale thin-films of APbI_3 ($\text{A}=\text{MA}^+$, FA^+ , MAFA^+ , CsMA^+ and CsMAFA^+) metal halide perovskites recrystallized from aprotic solvents DMF:DMSO (8:2) upon annealing at 120 °C.

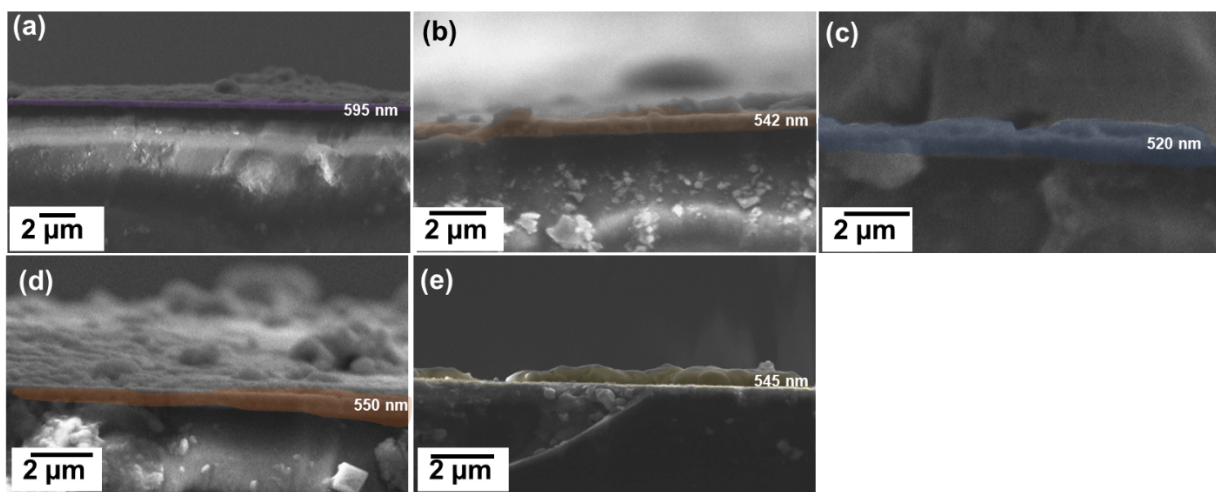


Fig S21. (a-e) SEM cross-sectional images of the as-prepared nanoscale thin-films of APbI_3 ($\text{A}=\text{MA}^+$, FA^+ , MAFA^+ , CsMA^+ and CsMAFA^+) metal halide perovskites recrystallized from aprotic solvents DMF:DMSO (8:2) upon annealing at 120 °C.

Table S5. Comparison of various memory device performance based on organic-inorganic metal halide perovskite materials

S.No	Device Structure	Endurance (Cycles)	Retention (s)	V_{SET}/V_{RESET} (V)	Ref	References
1.	FTO/TiO ₂ /MAPbI ₃ /Spiro-OmeTAD/Ag	2×10^2	2.4×10^4	0.8/-0.8	1	1. G. Landi, V. Subbiah, K. S. Reddy, A. Sorrentino, A. Samban dam, P. C. Ramam urthy and H. Neitzert, IEEE J. Electron Dev. Soc., 2018, 6 , 454–463 2. H. Cai, G. Ma, Y. He, C. Liu and H. Wang, <i>Org. Electron.</i> , 2018, 58 , 301–305. 3. Y. Ren, H. Ma, W. Wang, Z. Wang, H. Xu, X. Zhao, W. Liu, J. Ma and Y. Liu, <i>Adv. Mater. Technol.</i> , 2019, 4 , 1970004 4. W. Wang, J. Xu, H. Ma, X. Zhao, Y. Lin, C. Zhang, Z. Wang, H. Xu and Y. Liu, <i>ACS Appl. Nano Mater.</i> , 2019, 2 , 307–314. 5. Y. He, G. Ma, X. Zhou, H. Cai, C. Liu, J. Zhang and H. Wang, <i>Org. Electron.</i> , 2019, 68 , 230–235.
2.	FTO/MAPbI ₃ /W	10^2	-	3.1/-1.1	2	
3.	FTO/MAPbI ₃ /Al	10^3	-	1.5/-1.4	3	
4.	FTO/MAPbI ₃ /AgInSbTe/Al	1.2×10^2	10^4	0.5/-0.3	4	
5.	FTO/Zr-MAPbI ₃ /Pt	5×10^2	10^4	1.8/-1.3	5	
6.	FTO/MAPbBr ₃ /Ag	250	10^3	0.7/-0.3	6	
7.	FTO/MAPbBr _{2.54} Cl _{0.46} /Ag	250	10^3	0.8/-1.3	6	
8.	FTO/MAPbBr _{2.54} Cl _{0.46} /Ag	250	10^3	0.23/-3	6	
9.	FTO/MAPbI ₃ /Au	100	10^4	1/-1	7	
10.	FTO/CsPbBr ₃ /Au	100	3×10^3	1.5/-1.2	8	
11.	FTO/MAPI/Ag	1500	3×10^4	0.6/-0.8	This Work	C.
12.	FTO/FAPI/Ag	1200	2×10^4	0.7/-2.4	This Work	Ramam urthy
13.	FTO/MAFAPI/Ag	1300	2×10^4	0.5/-0.7	This Work	and H. Neitzert,
14.	FTO/CsMAPI/Ag	3500	6×10^4	0.3/-0.6	This Work	IEEE J. Electron Dev. Soc.,
15.	FTO/CsMAFAPI/Ag	5000	6×10^4	0.2/-0.6	This Work	

2018, **6**, 454–463

2. H. Cai, G. Ma, Y. He, C. Liu and H. Wang, *Org. Electron.*, 2018, **58**, 301–305.
3. Y. Ren, H. Ma, W. Wang, Z. Wang, H. Xu, X. Zhao, W. Liu, J. Ma and Y. Liu, *Adv. Mater. Technol.*, 2019, **4**, 1970004
4. W. Wang, J. Xu, H. Ma, X. Zhao, Y. Lin, C. Zhang, Z. Wang, H. Xu and Y. Liu, *ACS Appl. Nano Mater.*, 2019, **2**, 307–314.
5. Y. He, G. Ma, X. Zhou, H. Cai, C. Liu, J. Zhang and H. Wang, *Org. Electron.*, 2019, **68**, 230–235.

6. C. Muthu , S. Agarwal , A. Vijayan , P. Hazra , K. B. Jinesh and V. C. Nair , *Adv. Mater. Interfaces*, 2016, **3** , 1600092
7. Y. Wu , Y. Wei , Y. Huang , F. Cao , D. Yu , X. Li and H. Zeng , *Nano Res.*, 2017, **10** , 1584
8. H. Ma, W. Wang, H. Xu, Z. Wang, Y. Tao, P. Chen, W. Liu, X. Zhang, J. Ma and Y. Liu, *ACS Appl. Mater. Interfaces*, 2018, **10**, 21755–21763